Int J Adv Manuf Technol (2015) 79:1109–1116
DOI 10.1007/s00170-015-6874-z

ORIGINAL ARTICLE

Microstructural aspects in Al–Cu dissimilar joining by FSW

Pierpaolo Carlone · Antonello Astarita · Gaetano S. Palazzo · Valentino Paradiso · Antonino Squillace

Received: 4 August 2014 / Accepted: 2 February 2015 / Published online: 25 February 2015

Abstract Sound AA2024-T3–Cu10100 dissimilar joints were obtained by friction stir welding offsetting the tool probe towards the aluminum sheet and employing selected processing parameters. Joint microstructure was analyzed by means of conventional optic microscopy as well as scanning electron microscopy. The weld bead exhibited welding zones and some features typically encountered in similar FSW. The nugget zone consisted of a mixture of recrystallized aluminum matrix and deformed and twinned copper particles. Onion rings and particle-rich zones, made of Cu particles dispersed in the Al matrix, were also observed. EDS analysis revealed that several Al–Cu intermetallic compounds, such as Al_2Cu, AlCu, and Al_3Cu_4, chemically different w.r.t. compounds precipitated during the T3 aging treatment (Al_3Cu), were formed during the process. Microstructure variation significantly affects the microhardness distribution in the cross-section of the joint.

Keywords Friction stir welding · Dissimilar joint · AA2024-T3 · Cu10100 · Microstructure · EDS

1 Introduction

Dissimilar joining of aluminum to copper is gaining a great deal of attention in several applicative sectors. The intriguing advantages achievable in terms of weight saving and cost reduction make this combination of materials very appealing for the chemical, aerospace, transportation, and electronic industries [1–3]. Due to the difficulties in making an electrically stable bolted hybrid joint, much effort has been focused on welding aluminum to copper in the last decades [4].

Previous literature [5] pointed out that the joining of such dissimilar materials by fusion welding processes is quite challenging due to their different chemical, mechanical, and thermal properties. The melting points of aluminum and copper differ of about nearly 400 °C. This may result in remarkable non-homogeneities in the microstructure of the adjoined materials, negatively affecting the overall joint performance. Indeed, aluminum is easily oxidized at elevated temperatures, and welding cracks are commonly detected in brazed or fusion-welded Cu joints [6]. What is more, during fusion welding or pressure welding (brazing, diffusion bonding, etc) of Cu–Al some issues concerning the formation of hard and brittle intermetallic compounds (IMCs) in large scale at weld interface were highlighted by the experimental analysis reported by Liu et al. [7]. These IMCs could lead to a decreasing of the mechanical properties of the entire joint [8].

In recent years, solid-state joining techniques, such as friction welding, roll welding, and explosive welding, have received much interest for such applications [9–11]. Among others, a great deal of attention is directed towards the friction stir welding process (FSW). Some researchers studied the FSW of Al–Cu dissimilar joints, focusing on pure aluminum and cast aluminum alloys [12]. The literature converges on two general aspects: i. sound dissimilar FSW Al–Cu joints are difficult to achieve and ii. a key role is played by the brittle IMCs formed in the nugget zone (NZ). According to the experimental analysis performed by Murr et al. [3], Al–Cu joints generally fail at the NZ or along the interface between the two materials during the mechanical tests [13]. Ouyang et al. [1] attributed the poor weldability to various brittle IMCs formed in the NZ. Lee and Jung [14] suggested that the formation of Al_2O_3 and CuO layers resulted in lower tensile strength attributable to the presence of brittle IMCs. In a previous study [15], sound FSW Al–Cu joints were obtained by offsetting the tool to the aluminum side under a lower heat input condition. The formation of a thin, continuous, and uniform IMC layer created an excellent metallurgical bonding at Al–Cu interface,

P. Carlone (✉) · G. S. Palazzo
Department of Industrial Engineering, University of Salerno, Via Giovanni Paolo II 132, 84084 Fisciano, SA, Italy
e-mail: pcarlone@unisa.it

A. Astarita · V. Paradiso · A. Squillace
Department of Chemical, Materials and Industrial Production Engineering, University of Naples "Federico II", P.le Tecchio 80, 80100 Naples, Italy

and no oxide layer was found. It is well documented that several parameters, such as tool offsetting, rotation rate, and traverse speed, influenced the weld properties of the dissimilar FSW joints [16–19]. Despite the number of articles available on this topic, there are very few papers dealing with the dissimilar welding between copper and the high-strength aluminum alloys, such as 2XXX (Al–Cu) series. In particular, the AA2024 Al-Cu alloy is widely used for structural application in aeronautics [20, 21]. Due to the presence of copper precipitates at the grain boundaries, this alloy is expected to easily form IMCs with the copper during the FSW process. Moreover, its hardening mechanism is based on the formation of Al–Cu precipitates (in particular Al_3Cu) in the Al lattice, preventing the dislocations migration and enhancing the mechanical properties [22]. This paper studies the dissimilar joining by FSW between pure copper (Cu10100) and the high-strength aluminum alloy AA2024-T3. Due to the aforementioned reasons, the AA2024–Cu10100 joining by FSW is expected to produce a weld bead with a very complex metallurgy. The aims of this paper are to prove the capability of the FSW process to provide sound joints and to study the microstructure and the metallurgy of the joint.

2 Experimental

AA2024-T3 rolled sheet and pure Cu10100 rolled and cold drawn sheet were used as base material. The chemical composition and the main mechanical properties of the two alloys are fully available elsewhere [23, 24] and are not reported here in the interest of brevity. Dimensions of the adjoined sheets were 120 mm (length), 30 mm (width), and 2 mm (thickness). AA2024 sheet was fixed in the advancing side of the joint and the tool was displaced towards the aluminum side (i.e., the harder material) of a predefined offset. A scheme of the welding configuration, including also a detail of the tool, is provided in Fig. 1.

Non-consumable tools, made of Cr-Mo steel, were used to fabricate the joints. Tool geometry is characterized by a shoulder diameter of 20 mm and by an unthreaded conical probe with 5.2-mm major diameter, 15° cone angle, and 1.8-mm length. The forging action of the tool shoulder was enhanced imposing a tilt angle of 2°. Process parameters were chosen on the basis of the available literature and comparing the process windows obtained welding singularly AA2024-T3 and Cu10100 [25, 26]. Furthermore, a preliminary test campaign was performed by trial and error before the achievement of material continuity. The employed parameters are given in Table 1.

The welding process was carried out following plunging, dwelling, and welding phases. The feed rate of the tool along the vertical axis during the plunging phase was set as 5 mm/min, while the duration of dwell was set as 10 s. Three different joints were carried out in order to ensure the repeatability of the process. The microstructure of the joint was studied through metallographic observations by means of both light optical microscope and scanning electron microscope (SEM). Moreover, chemical composition measurements were carried out through an EDS probe to study the IMCs generated by the welding process. In more details, each specimen was cold mounted in a proper thermoset resin and polished with grinding discs (P320, P600, P1200, P2000) and polycrystalline diamond suspension (3 μm) on tissue disc until the surface exhibited a mirror like finish. Afterwards, the samples were etched by a modified Keller's reagent (150 ml H_2O, 2 ml HNO_3, 6 ml HCl, 6 ml HF) to unveil the significant features of the aluminum metallurgical microstructures. The same procedure was repeated to investigate the copper microstructures using a solution of 30 ml HCl, 40 ml HNO_3, 2.5 ml HF, 12 g C_2O_2, and 42.5 ml H_2O. Optical observations were performed using a metallurgical microscope equipped with a digital camera to evaluate the weld bead morphology. SEM observations and EDS measurements were carried out through a table top SEM equipped with an EDS probe. Vickers microhardness was measured in the cross-section of the joint in order to assess the influence of the microstructure on the mechanical properties of the joint itself. Three linear patterns, orthogonal to the weld line, were programmed, respectively, at the mid-thickness of the joint cross-section and at a distance equal to 0.5 mm towards the top and bottom surfaces. The following parameters were adopted: distance between two consecutive indentations 1 mm, indentation load 50 gf (0.49 N), loading time 15 s, and indentation speed 60 μm/s.

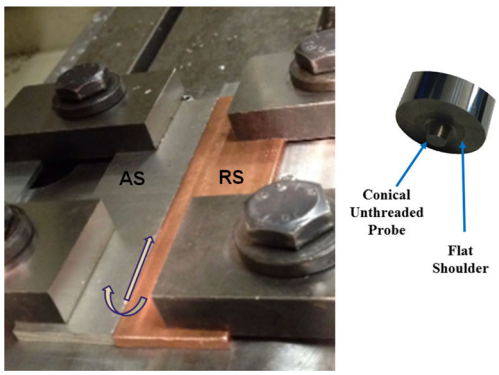

Fig. 1 FSW process setup and tool

3 Results and discussion

The surface morphology of the joint is shown in Fig. 2. Sound weld surfaces were achieved adopting the aforementioned

Table 1 FSW process parameters

Rotational speed (rpm)	Welding speed (mm/min)	Tilt angle (°)	Tool offset (mm)
1000	80	2	1.3

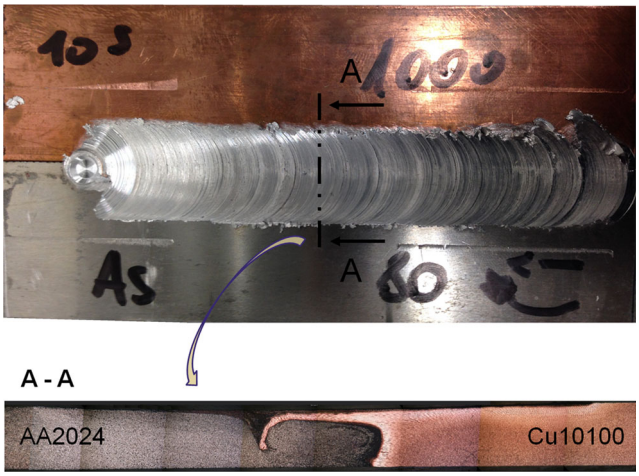

Fig. 2 Surface morphology of the joint (*top*) and cross-section macrograph of the joint (*bottom*)

welding configuration and parameters. In this regard, it is worth to point out that in preliminary FSW tests, tunnel defects, as well as surface defects (i.e., groove, flash, instability of the welding path), were observed reverting the position of the two sheets even reducing the welding speed. Figure 2 shows also the cross-sectional macrograph obtained after etching. Satisfactory material continuity was exhibited in the weld bead. The stirring experienced by the material during the process is well appreciable in the same figure. As can be seen, copper exhibits a higher deformation with respect to aluminum. Indeed, the softened copper, stirred by the probe action, penetrates into the aluminum sheet. During FSW process, adjoining material is transferred from the retreating side to the advancing side behind the probe, where the weld bead is formed [27, 28]. When the softer material is fixed at the retreating side, it is easily forced towards the advancing side. Being the hardness of the AA2024 higher than that of the Cu10100, an enhanced material flow in the soft copper base is reasonably expected [29]. The plastic flow of the copper is clearly evident looking at the remixed copper hook in Fig. 2, creating a sort of mechanical bond between the two materials. This allows affirming that fixing the harder plate (AA 2024 in this study) in the advancing side of the joint during dissimilar FSW is one of the key factors providing sound weld quality. Previous studies indicated that the weld quality in dissimilar FSW joints is strongly influenced by the offsetting of the probe [30]. Similar considerations apply to other materials pairs. For instance, Watanabe et al. [17] reported that long crack lines were observed on the crown of FSW Al–Fe joints when the Fe (i.e., the harder material) was fixed in the retreating side and sound weld surface could be obtained in reversed fixing conditions.

Figure 3 shows the SEM macroscopic appearance and microstructures of the Al–Cu joint. The NZ consists of a mixture of aluminum matrix and Cu particles. Many fine particles with various sizes and irregular shapes were dispersed in the Al matrix; large particles were also observed. The distribution of Cu particles appeared inhomogeneous in the NZ and a particles-rich zone (PRZ) was also detected near the bottom. Thus, the NZ can be considered an aluminum matrix composite with both Cu particles and Al–Cu intermetallic dispersed within. The presence of this structure is attributable to the stirring action of the tool probe, which scraped Cu pieces from the bulk copper, breaking up and dispersing them during FSW process. Typical onion rings, made of Cu particles dispersed in the Al matrix, were also detected. Intriguingly, a remixing zone (RZ) resembling the typical thermo-mechanically affected zone (TMAZ) observed in similar FSW butt joints was individuated (Fig. 3) and related to diffusion phenomena induced by thermo-mechanical loads experienced by the adjoining materials.

In Figure 4, microstructures observed in the stirred materials (points 1 and 2, as indicated in Fig. 3) as well as in the undeformed base materials (point 3 and 4, as indicated in Fig. 3) are reported. Figure 4.1 depicts the microstructure in the NZ. In this zone, due to the thermo-mechanical action of the tool, the microstructure was fully recrystallized resulting in the fine equiaxial grains with average grain diameter equal to 30 μm. In Fig. 4.2, the microstructure observed in the point 2 of Fig. 3 is reported. In these zone, copper experienced a severe plastic flow but the heat input was too low to achieve a fully recrystallization. As a consequence, the mean grain dimension was similar to the one of the parent material, with

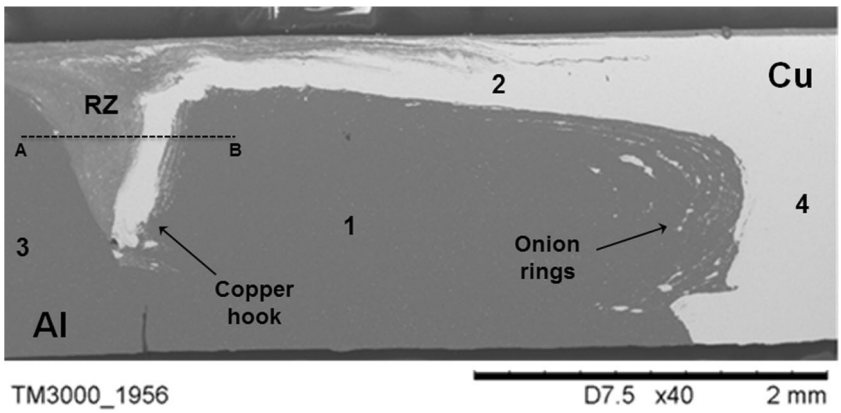

Fig. 3 SEM macrograph of the cross-section of the weld bead

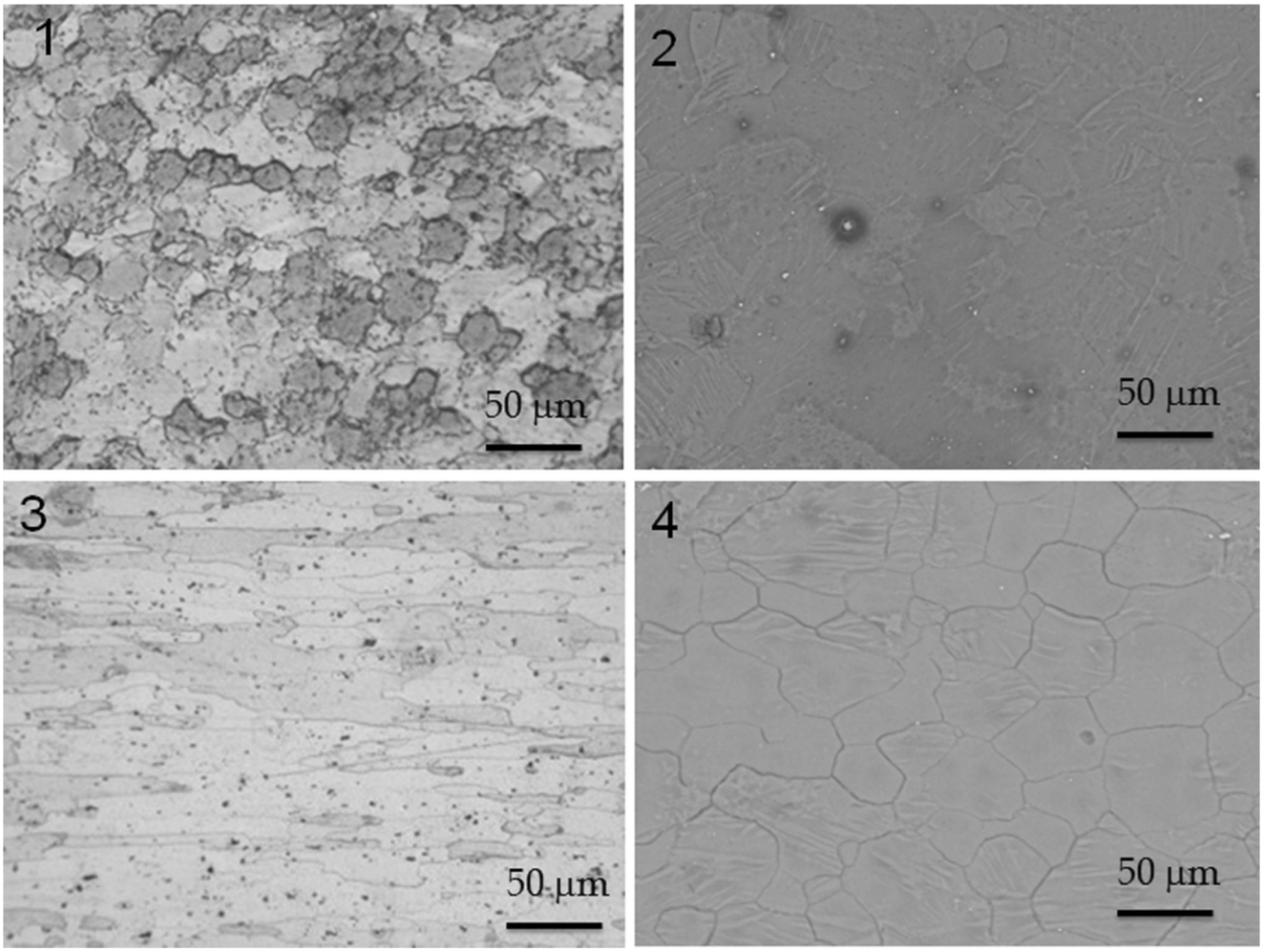

Fig. 4 Microstructure of joint. NZ (*1*), deformed Cu (*2*), undeformed AA2024-T3 (*3*), undeformed Cu10100 (*4*)

an average diameter of approximately 50 μm. However, the stirring effect induced very deformed and twinned grains, characterized by low-defined borders. Concerning the Al in the zone external to the weld bead (Fig. 4.3), it is appreciable the typical microstructure of the rolled AA2024 after the T3 aging treatment. Pancake-elongated grains were exhibited, with the presence of the Al_3Cu precipitates. Moreover, second-phase black particles were also visible, exhibiting typical composition encountered in 2XXX aluminum alloys (that is rich in Fe, Cu, Mg, and Mn). The microstructure of the Cu10100, externally to the stirred zone, showed the typical features induced by the cold drawing process, with the presence of some deformed grains (Fig. 4.4).

As far IMCs precipitation is regarded, the Al–Cu binary equilibrium phase diagram [31] clearly indicates that several Al–Cu particles, including Al_2Cu, AlCu, and Al_3Cu_4, may be developed during the Al/Cu process-induced reaction. Some studies discussed that Al-rich phase Al_2Cu and Cu-rich phase Al_4Cu_9 were the first two IMCs formed adjacent to Al side and Cu side, respectively [32–34]. However, it should be borne in mind that the AA2024 base material used in this work was rich of Al_3Cu precipitates due to the T3 heat treatment, so it is important to distinguish these particles from IMCs developed during the welding process. SEM images depicting observed IMCs are reported in Fig. 5. The presence of the above-cited IMCs in the NZ was clearly highlighted by the position and the energy intensity of peaks measured by EDS (shown in Fig. 6) and the analysis of their chemical composition, in terms of atomic percentage, (given in Table 2). Performed SEM/

Table 2 Chemical composition, in terms of atomic percentage, of IMCs precipitated during FSW process and detected in the NZ

IMC	Al (%)	Cu (%)
AlCu	52	48
Al_2Cu	65	35
Al_3Cu_4	42	58
Al_3Cu	76	24

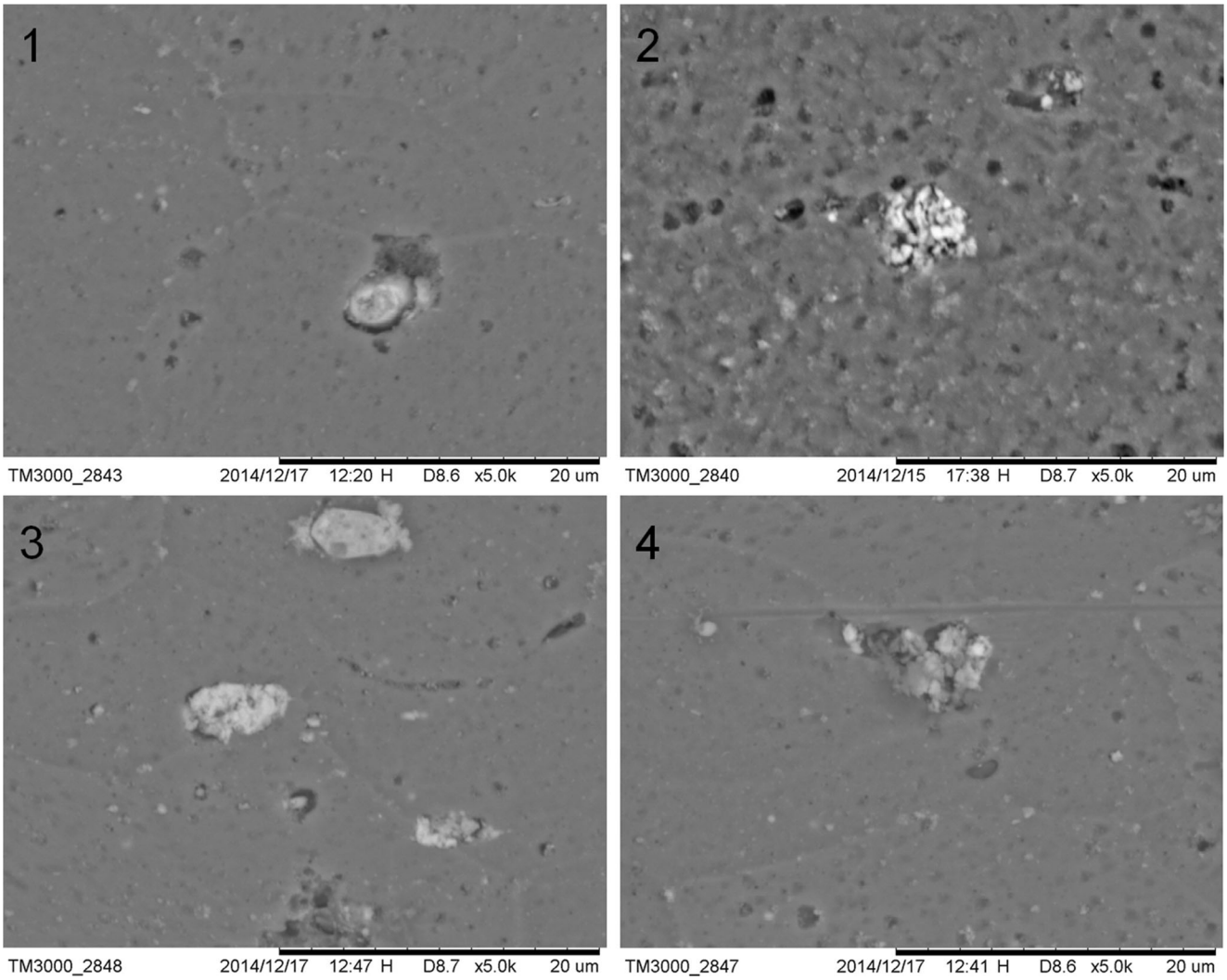

Fig. 5 Images of IMCs observed by SEM analysis. AlCu (*1*), Al_2Cu (*2*), Al_3Cu_4 (*3*), Al_3Cu (*4*)

EDS analysis pointed out the presence of IMCs in the aluminum matrix constituting the NZ, as well as their total absence in the copper surrounding or dispersed in the NZ. Indeed, the temperature experienced by the materials during the process was not sufficient to induce an actual recrystallization of the Cu microstructure. What is more, the relatively fast cooling of the materials pair prevented the precipitation of IMC in copper.

As aforementioned, these particles affect the mechanical behavior of the joint [35, 36]. The EDS analysis also confirmed that these particles differ from the Al_3Cu particles precipitated during the aging phase of the heat treatment (Fig. 6.4). The chemical composition of these particles (Al_2Cu, AlCu, Al_3Cu_4) is given in Table 2. In Fig. 7, a magnification of the PRZ zone is reported, showing several Cu particles dispersed in the aluminum matrix.

Figure 8 shows aluminum and copper intensity, as measured through EDS analysis, along the scan line AB, as depicted in Fig. 3. Please note that intensity values were normalized for both elements with respect to the maximum peak intensity in order to improve the readability of the plot. The variability of the presence of aluminum and copper can be well appreciated, confirming that in this zone, the stirring action induced an intimately remixing between the two materials and a quite non-homogeneous microstructure. More specifically, at the beginning of the scan line, in correspondence of the undeformed aluminum, the chemical composition reflects the typical AA2024 one. Al percentage gradually drops with a contemporary increase of the Cu percentage approaching the RZ. Some abnormal peaks in the copper profile evidence the presence of large copper particles or lamellae dispersed in the aluminum. Then, a segment characterized by the predominant presence of copper is encountered, corresponding to the copper hook. As shown, the aluminum content completely vanishes, confirming that this hook was roughly created by the copper stirred and deposed on the advancing side of the weld.

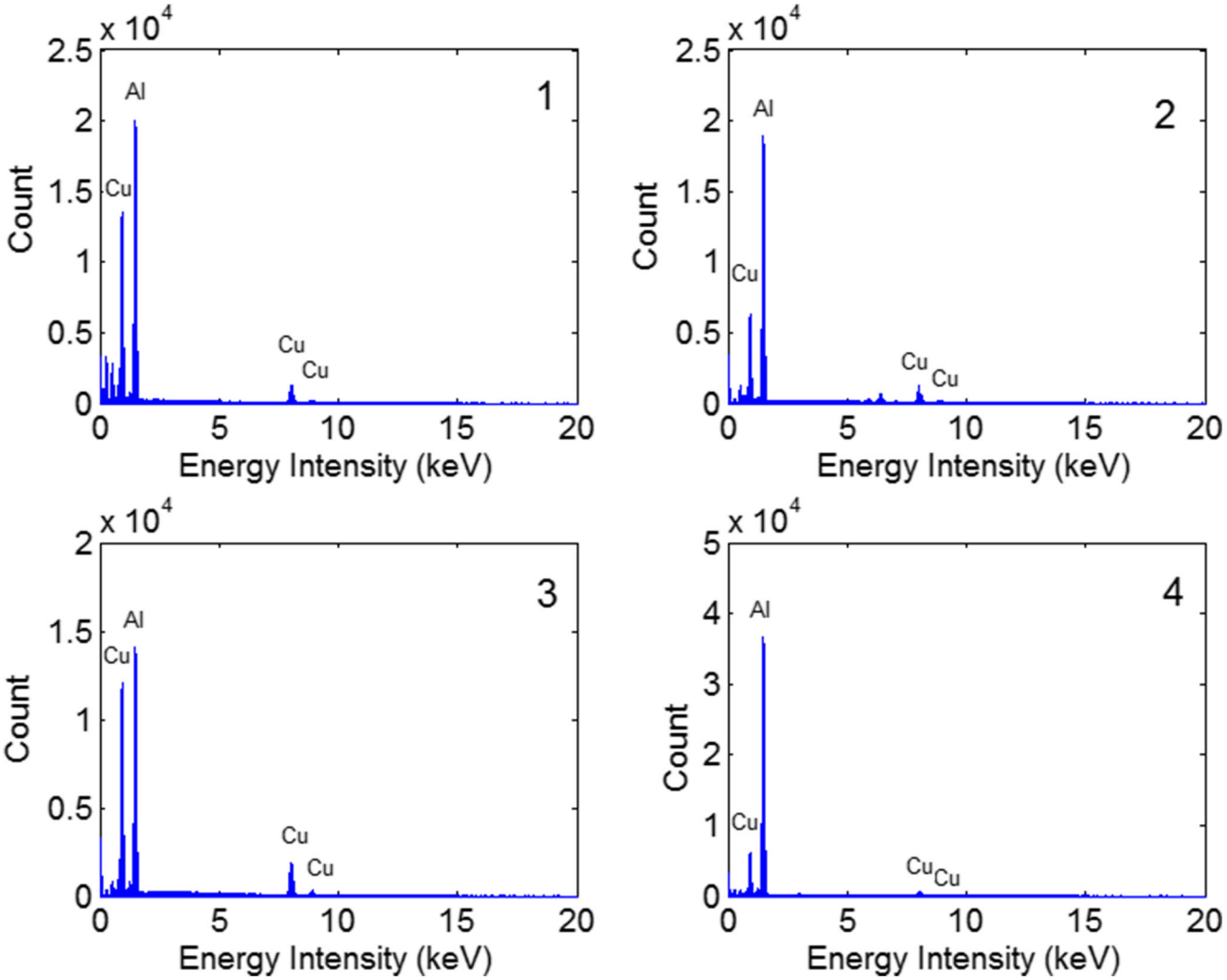

Fig. 6 IMCs intensity peaks provided by EDS analysis. AlCu (*1*), Al_2Cu (*2*), Al_3Cu_4 (*3*), Al_3Cu (*4*)

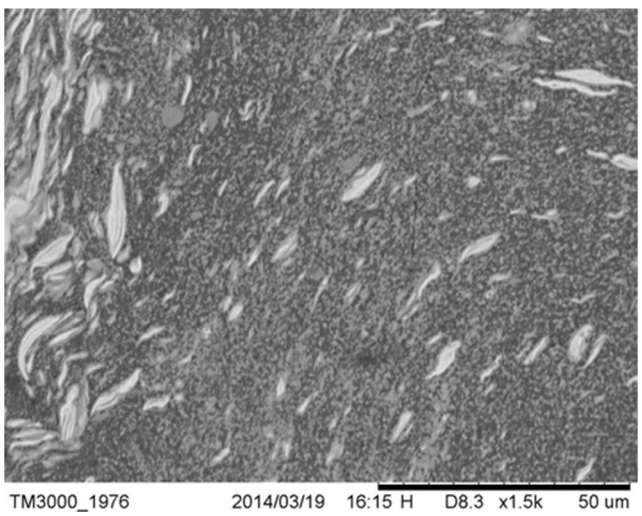

Fig. 7 Magnification of the PRZ zone (Cu particles are *brighter* than the Al matrix)

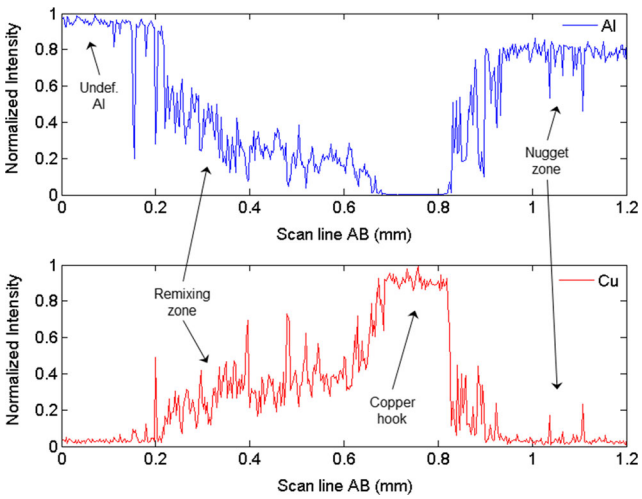

Fig. 8 Al and Cu intensity, as measured along the line AB depicted in Fig. 3

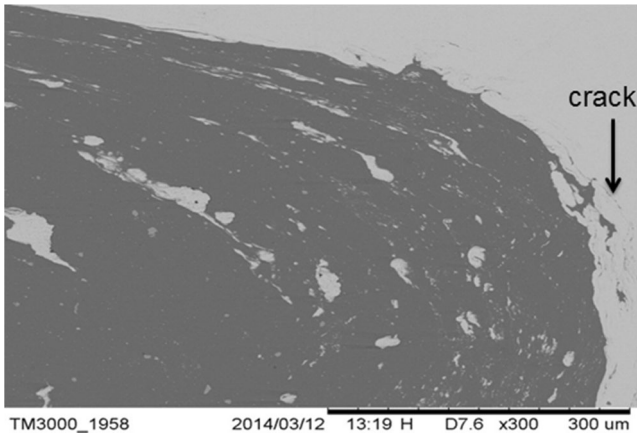

Fig. 9 Interface between AA2024 and Cu10100 (copper is *brighter*)

Beyond this formation, Al content increases and Cu content decreases following a marked oscillating behavior, resembling sort of a layered Al–Cu deposition. Finally, in the NZ, aluminum content results minor with respect to the parent material, due to the copper particles dispersed therein.

In Fig. 9, a micrograph of transition zone in the retreating (copper) side is reported. Some cracks due to the stirring and scratching action of the probe are appreciable. As generally accepted, the presence of these cracks reduces the mechanical properties of the joint; however, they are also recognized as a peculiar feature of this kind of dissimilar joints [16].

The microhardness distribution mapped in Fig. 9 highlights the influence of the process-induced microstructure on the local mechanical properties of the joint. The transition between the AA2024 base material and the Cu10100 base material is clearly visible in correspondence of the weld line. A sharp microhardness increase was evaluated in the NZ. Microhardness increase is well justified observing the subfigure included in Fig. 10, reporting the aluminum energy intensity measured by SEM/EDS along a scan line transverse to the nugget zone. As can be seen, aluminum content is the main factor dictating the microhardness distribution. What is more, despite of the grain refinement, microhardness values minor than the base material were exhibited, due to the copper particles dispersed within. Some peaks were also measured, attributable to the intermetallic particles observed in the joint.

4 Conclusions

On the basis of the experimental campaign carried out, the following consideration could be drawn:

- Sound AA2024-Cu10100 joints can be obtained by FSW offsetting the probe towards the aluminum side and fixing the copper in the retreating zone.
- The final microstructure exhibits typical FSW features. The NZ consists of a mixture of recrystallized aluminum matrix and deformed/twinned copper particles, resembling an aluminum matrix composite. The distribution of Cu particles with irregular shapes and various sizes appeared inhomogeneous in the NZ, with the formation of a particles-rich zone near the bottom. Onion rings, made of Cu particles dispersed in the Al matrix, were also observed.
- EDS analysis evidenced the presence of Al–Cu IMCs, namely, Al_2Cu, AlCu, and Al_3Cu_4, developed during the welding process. The chemical composition of these

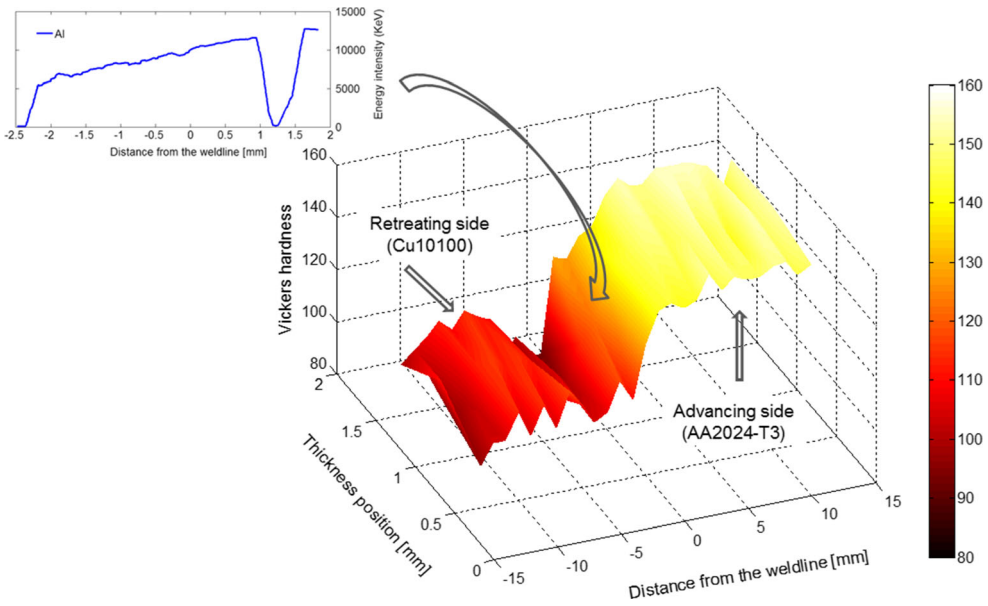

Fig. 10 Microhardness map in the weld bead, including an EDS analysis along a scan line transverse to the NZ

particles is in accordance with the Al–Cu binary equilibrium phase diagram.

– A sharp microhardness increase was measured in the NZ, consistently with the observed microstructure. In particular, the aluminum content appears as a dominant factor influencing the local microhardness value.

References

1. Ouyang J, Yarrapareddy E, Kovacevic R (2006) Microstructural evolution in the friction stir welded 6061 aluminum alloy (T6-temper condition) to copper. J Mater Process Technol 172:110–122
2. Murr LE, Flores RD, Flores OV, McClure JC, Liu G, Brown D (1998) Friction stir welding: microstructural characterization. Mater Res Innovation 1(4):211–223
3. Murr LE, Ying L, Trillo EA, Flores RD, McClure JC (1998) Microstructure in friction stir welded metals. J Mater Process Manuf Sci 7:145–161
4. Dawes CJ (1977) Micro-friction welding aluminum studs to mild steel plates. Met Constr 9(5):196–197
5. Sun Z, Karppi R (1996) The application of electron beam welding for the joining of dissimilar metals: an overview. J Mater Process Technol 59:257–267
6. Aravind M, Yu P, Yau MY, Dickon HLN (2004) Formation of Al_2Cu and AlCu intermetallics in Al(Cu) alloy matrix composites by reaction sintering. Mater Sci Eng A 380:384–393
7. Liu P, Shi Q, Wang W, Wang X, Zhang Z (2008) Microstructure and XRD analysis of FSW joints for copper T2/aluminium 5A06 dissimilar materials. Mater Lett 62:4106–4108
8. Galvão I, Oliveira JC, Loureiro A, Rodrigues DM (2012) Formation and distribution of brittle structures in friction stir welding of aluminium and copper: Influence of shoulder geometry. Intermetallics 22: 122–128
9. Abbasi M, Karimi Taheri A, Salehi MT (2001) Growth rate of intermetallic compounds in Al/Cu bimetal produced by cold roll welding process. J Alloy Compd 319:233–241
10. Squillace A, De Fenzo A, Giorleo G, Bellucci F (2004) A comparison between FSW and TIG welding techniques: modifications of microstructure and pitting corrosion resistance in AA 2024-T3 butt joints. J Mater Process Technol 152(1):97–105
11. Mofid MA, Abdollah-Zadeh A, Gür CH (2014) Investigating the formation of intermetallic compounds during friction stir welding of magnesium alloy to aluminum alloy in air and under liquid nitrogen. Int J Adv Manuf Technol 71(5–8):1493–1499
12. Yilbas BS, Sahin AZ, Kahraman N, Al-Garni AZ (1995) Friction welding of steel–Al and Al–Cu materials. J Mater Process Technol 49:431–443
13. Midling OT, Grong Ø (1994) A process model for friction welding of Al–Mg–Si alloys and Al–SiC metal matrix composites-I. HAZ temperature and strain rate distribution. Acta Metall Mater 42(5):1595–1609
14. Lee WB, Jung SB (2003) Void free friction stir weld zone of the dissimilar 6061 aluminum and copper joint by shifting the tool insertion location. Mater Res Innov 8(2):93–96
15. Pratik Agarwal S, Prashanna Nageswaran, Arivazhagan N, Devendranath Ramkumar K (2012) Development of friction stir welded butt joints of AA 6063 aluminium alloy and pure copper. In Proceedings of the International Conference on Advanced Research in Mechanical Engineering (ICARME-2012) 13 May 2012, Trivendum, India
16. Saeid T, Abdollah-zadeh A, Sazgari B (2010) Weldability and mechanical properties of dissimilar aluminum–copper lap joints made by friction stir welding. J Alloy Compd 490:652–655
17. Watanabe T, Takayama H, Yanagisawa A (2006) Joining of aluminum alloy to steel by friction stir welding. J Mater Process Technol 178:342–349
18. Tanaka T, Morishige T, Hirata T (2009) Comprehensive analysis of joint strength for dissimilar friction stir welds of mild steel to aluminum alloys. Scripta Mater 61:756–759
19. DebRoy T, Bhadeshia HKDH (2010) Friction stir welding of dissimilar alloys—a perspective. Sci Technol Weld Joining 15:266–270
20. Choi DH, Lee CY, Ahn BW, Yeon YM, Park SHC, Sato YS, Kokawa H, Jung SB (2010) Effect of fixed location variation in friction stir welding of steels with different carbon contents. Sci Technol Weld Joining 15:299–304
21. Hussain G, Gao L, Hayat N, Dar NU (2010) The formability of annealed and pre-aged AA-2024 sheets in single-point incremental forming. Int J Adv Manuf Technol 46(5–8):543–549
22. ASM Handbook, Volume 04 - Heat Treating
23. ASM Specialty Handbook: Aluminum and Aluminum Alloys
24. ASM Specialty Handbook—Copper and Copper Alloys
25. Carlone P, Palazzo GS (2013) Influence of process parameters on microstructure and mechanical properties in AA2024-T3 friction stir welding. Metallogr Microstruct Anal 2(4):213–222
26. Carlone P, Palazzo GS (2014) The influence of pre-heating on the weldability of pure copper by FSW. Open Mech Eng J 8:177–184
27. Nandan R, DebRoy T, Bhadeshia HKDH (2008) Recent advances in friction-stir welding—process, weldment structure and properties. Prog Mater Sci 3:980–1023
28. Reynolds AP (2008) Flow visualization and simulation in FSW. Scripta Mater 58:338–342
29. Xue P, Ni DR, Wang D, Xiao BL, Ma ZY (2011) Effect of friction stir welding parameters on the microstructure and mechanical properties of the dissimilar Al–Cu joints. Mater Sci Eng A 528:4683–4689
30. Tolephih MH, Mahmood HM, Hashem AH, Abdullah ET (2013) Effect of tool offset and tilt angle on weld strength of butt joint friction stir welded specimens of AA2024 aluminum alloy welded to commercial pure cupper. Chem Mater Res 3(4):49–58
31. Massalski TB (1980) The Al–Cu (aluminum-copper) system. Bull Alloy Phase Diagr 1(1):27–33
32. Chen CY, Chen HL, Hwang WS (2006) Influence of interfacial structure development on the fracture mechanism and bond strength of aluminum/copper Bimetal Plate. Mater Trans JIM 47:1232–1239
33. Jiang HG, Dai JY, Tong HY, Ding BZ, Song QH, Hu ZQ (1993) Interfacial reactions on annealing Cu/Al multilayer thin films. J Appl Phys 74:6165–6169
34. Peng XK, Wuhrer R, Heness G, Yeung WY (1999) On the interface development and fracture behaviour of roll bonded copper/aluminium metal laminates. J Mater Sci 34:2029–2038
35. Won-Bae L, Yun-Mo Y, Seung-Boo J (2003) The joint properties of dissimilar formed Al alloys by friction stir welding according to the fixed location of materials. Scripta Mater 49:423–428
36. Xue P, Xiao BL, Ni DR, Ma ZY (2010) Enhanced mechanical properties of friction stir welded dissimilar Al–Cu joint by intermetallic compounds. Mater Sci Eng A 527:5723–5727